

Neuroimaging

Regional tau deposition and subregion atrophy of medial temporal structures in early Alzheimer's disease: A combined positron emission tomography/magnetic resonance imaging study

Daichi Sone<sup>a,b</sup>, Etsuko Imabayashi<sup>a</sup>, Norihide Maikusa<sup>a</sup>, Nobuyuki Okamura<sup>c,d</sup>, Shozo Furumoto<sup>e</sup>, Yukitsuka Kudo<sup>d</sup>, Masayo Ogawa<sup>a</sup>, Harumasa Takano<sup>f</sup>, Yuma Yokoi<sup>f</sup>, Masuhiro Sakata<sup>f</sup>, Tadashi Tsukamoto<sup>g</sup>, Koichi Kato<sup>a</sup>, Hiroshi Matsuda<sup>a,\*</sup>

<sup>a</sup>Integrative Brain Imaging Center, National Center of Neurology and Psychiatry, Tokyo, Japan

<sup>b</sup>Department of Neuropsychiatry, Graduate School of Medicine, The University of Tokyo, Tokyo, Japan

<sup>c</sup>Division of Pharmacology, Faculty of Medicine, Tohoku Medical and Pharmaceutical University, Sendai, Japan

<sup>d</sup>Division of Neuro-imaging, Institute of Development, Aging and Cancer, Tohoku University, Sendai, Japan

<sup>e</sup>Division of Radiopharmaceutical Chemistry, Cyclotron and Radioisotope Center, Tohoku University, Sendai, Japan

<sup>f</sup>Department of Psychiatry, National Center of Neurology and Psychiatry, Tokyo, Japan

<sup>g</sup>Department of Neurology, National Center of Neurology and Psychiatry, Tokyo, Japan

Abstract

**Introduction:** Molecular imaging and selective hippocampal subfield atrophy are a focus of recent Alzheimer's disease (AD) research. Here, we investigated correlations between molecular imaging and hippocampal subfields in early AD.

**Methods:** We investigated 18 patients with early AD and 18 healthy control subjects using <sup>11</sup>C-Pittsburgh compound-B (PIB) positron emission tomography (PET) and <sup>18</sup>F-THK5351 PET and automatic segmentation of hippocampal subfields with high-resolution T2-weighted magnetic resonance imaging. The PET images were normalized and underwent voxelwise regression analysis with each subregion volumes using SPM12.

**Results:** As for <sup>18</sup>F-THK5351 PET, the bilateral perirhinal cortex volumes were significantly associated with the ipsilateral or bilateral temporal lobar uptakes, whereas hippocampal subfields showed no correlations. <sup>11</sup>C-PIB PET showed relatively broad negative correlation with the right cornu ammonis 3 volumes.

**Discussion:** Regional tau deposition was correlated with extrahippocampal subregional atrophy and not with hippocampal subfields, possibly reflecting different underlying mechanisms of atrophy in early AD. Amyloid might be associated with right cornu ammonis 3 atrophy.

© 2017 The Authors. Published by Elsevier Inc. on behalf of the Alzheimer's Association. This is an open access article under the CC BY-NC-ND license (<http://creativecommons.org/licenses/by-nc-nd/4.0/>).

Keywords:

Tau PET; Hippocampal subfield; Alzheimer's disease; Entorhinal cortex; Perirhinal cortex

1. Introduction

Alzheimer's disease (AD) is the most common type of neurodegenerative dementia. Abnormal accumulations of extracellular amyloid  $\beta$  and intracellular neurofibrillary tangles (NFTs) of tau proteins are hallmarks of AD. Recently, AD research has begun taking advantage of various emerging advanced neuroimaging methods, with tau positron emission

The authors have no conflict of interest.

\*Corresponding author. Tel.: +81-042-341-2711; Fax: +81-042-344-6745.

E-mail address: [matsudah@ncnp.go.jp](mailto:matsudah@ncnp.go.jp)

<http://dx.doi.org/10.1016/j.dadm.2017.07.001>

2352-8729/© 2017 The Authors. Published by Elsevier Inc. on behalf of the Alzheimer's Association. This is an open access article under the CC BY-NC-ND license (<http://creativecommons.org/licenses/by-nc-nd/4.0/>).

tomography (PET) considered particularly promising for in vivo estimations of AD pathology [1]. A recent study revealed that tau PET uptake patterns strongly reflect regional associations with clinical and anatomic variability, whereas amyloid PET shows a more diffuse distribution and less regional associations with other parameters [2].

Hippocampal atrophy is a key structural imaging finding in AD [3]. The selectivity of hippocampal subfield atrophy has attracted attention for its diagnostic and predictive potential [4,5], and specific cortices such as the entorhinal cortex (ERC) and perirhinal cortex (PRC) are also considered important for memory networks [6,7].

Because tau deposition can potentially affect clinical and morphologic parameters in AD and medial temporal subregions may also have diagnostic and/or predictive value, investigation of the relationships between subregional atrophy and abnormal accumulations such as tau deposition is required. We conducted this study to explore imaging correlations using  $^{11}\text{C}$ -Pittsburgh compound-B (PIB) PET,  $^{18}\text{F}$ -THK5351 PET [8], and automatic segmentation of hippocampal subfields (ASHS) with high-resolution T2-weighted magnetic resonance imaging (MRI), which is a reliable method for subregional volumetry in various neurologic diseases [3,9,10].

## 2. Methods

### 2.1. Patients and control subjects

We recruited 18 Japanese patients (13 women, 5 men) with early AD at our institute. AD was diagnosed based on the clinical criteria for probable AD [11] and the presence of an abnormal cortical accumulation of amyloid revealed by the visual assessment of  $^{11}\text{C}$ -PIB PET images. The patients were  $70.3 \pm 8.5$  years old (mean  $\pm$  standard deviation [SD]), their average Mini-Mental State Examination (MMSE) score was  $22.6 \pm 4.1$  (mean  $\pm$  SD), and their global Clinical Dementia Rating ranged from 0.5 to 1.0. Almost all patients had less than 1 year disease duration except two patients with a few years' history from the diagnoses.

For reciprocal comparisons of abnormal depositions on PET and subregional atrophy, we also recruited 18 healthy Japanese control subjects (10 women, 8 men) with normal cognition who showed visually normal  $^{11}\text{C}$ -PIB and  $^{18}\text{F}$ -THK5351 PET results. The control subjects were  $66.8 \pm 9.5$  years old, with an average MMSE score of  $29.2 \pm 1.0$  and a global Clinical Dementia Rating of 0. There were no significant differences in the mean age or sex proportion between the early AD patient and healthy control groups. All clinical assessments and imaging scans were performed within a 12-week period.

All subjects gave written consent to participate in the study, which was approved by the Institutional Review Board at Japan's National Center of Neurology and Psychiatry.

### 2.2. Imaging acquisition

All participants underwent MRI scanning on a 3.0-T MRI system (Verio, Siemens, Erlangen, Germany). The sequence

parameters were as follows. Three-dimensional sagittal T1-weighted magnetization prepared rapid acquisition with gradient echo images: repetition time/echo time, 1900 ms/2.52 ms; flip angle,  $9^\circ$ ; in-plane resolution,  $1.0 \times 1.0$  mm; 1.0-mm effective slice thickness with no gap; 300 slices; matrix,  $256 \times 256$ ; field of view,  $25 \times 25$  cm; acquisition time, 4 minutes 18 seconds.

High-resolution T2-weighted images were designed for hippocampal subfield segmentation and obtained as follows: repetition time/echo time, 7380 ms/76 ms; flip angle,  $150^\circ$ ; in-plane resolution,  $0.4 \times 0.4$  mm; 2-mm slice thickness with no gap; 30 slices; matrix of  $512 \times 432$ ;  $22 \times 22$  cm field of view; acquisition time, 6 minutes 33 seconds.

All the PET/computed tomography (CT) scans were performed on a combined PET/CT scanner (Biograph 16; Siemens). For  $^{11}\text{C}$ -PIB imaging,  $^{11}\text{C}$ -PIB at a dose of 555 MBq was injected intravenously 50 minutes before the PET/CT scan, and the emission scan duration was 20 minutes. For  $^{18}\text{F}$ -THK5351 imaging,  $^{18}\text{F}$ -THK5351 at a dose of 185 MBq was injected 40 minutes before the scan, and the scan duration was 20 minutes. PET/CT images were reconstructed using a combination of Fourier rebinning and ordered subset expectation maximization.

### 2.3. ASHS volumetry of hippocampal and mesiotemporal subfields

We input both the T1- and high-resolution T2-weighted images obtained from all subjects into an open-source ASHS software program (<https://sites.google.com/site/hipposubfields/>) [9]. The "UPenn PMC Atlas" [9] was selected as the atlas set. The software calculated the volumes of each subfield fully automatically with a combination of multiatlas label fusion and learning-based error correction. The following 10 regions of interest were delineated: cornu ammonis (CA) 1, CA2, CA3, dentate gyrus (DG), subiculum, ERC, Brodmann area (BA) 35, BA36, collateral sulcus, and miscellaneous parts. Experienced neuroradiologists visually confirmed that the parcellation quality was good or fair.

### 2.4. PET normalization

After partial volume correction by PETPVE12 toolbox [12], both the  $^{11}\text{C}$ -PIB and  $^{18}\text{F}$ -THK5351 PET images were normalized using the statistical parametric mapping software 12 program (SPM12; <http://www.fil.ion.ucl.ac.uk/spm>). The subjects' T1-weighted images were coregistered to their PET images and normalized with diffeomorphic anatomic registration using the exponentiated lie method [13]. A transformation matrix was applied to each PET image, which had been coregistered to T1-weighted image through the partial volume correction process.

After spatial normalization, all the PET images were divided by the individual's positive mean uptake value of cerebellar gray matter. Finally, each PET image was smoothed by an 8-mm full width at half maximum Gaussian

Table 1

Volumes of the subregions in both the early AD patients and the healthy control subjects calculated by ASHS and the z-scores of the AD patients in each subregion

Left subregion	Volume (mm <sup>3</sup> )				z-score of AD	Right subregion	Volume (mm <sup>3</sup> )				z-score of AD
	AD	Control	P value				AD	Control	P value		
CA1	1002.3 ± 178.5	1338.4 ± 146.7	<.001	-2.29 ± 1.22	CA1	1007.2 ± 183.7	1397.5 ± 165.8	<.001	-2.35 ± 1.11		
CA2	12.5 ± 6.7	18.7 ± 7.3	.021	-0.86 ± 0.92	CA2	19.9 ± 4.9	23.9 ± 6.7	.063	-0.61 ± 0.73		
CA3	71.1 ± 17.2	67.5 ± 18.0	.435	0.20 ± 0.96	CA3	73.6 ± 14.1	70.2 ± 17.6	.825	0.20 ± 0.81		
DG	606.4 ± 116.3	817.3 ± 113.7	<.001	-1.85 ± 1.02	DG	608.7 ± 95.0	851.7 ± 107.0	<.001	-2.27 ± 0.89		
SUB	304.5 ± 67.3	391.2 ± 63.3	.002	-1.37 ± 1.06	SUB	298.3 ± 63.3	407.7 ± 74.3	<.001	-1.47 ± 0.85		
ERC	426.2 ± 97.4	504.9 ± 48.4	.024	-1.62 ± 2.01	ERC	390.7 ± 111.3	510.1 ± 62.3	.002	-1.92 ± 1.79		
BA35	340.7 ± 65.4	429.5 ± 97.9	.015	-0.91 ± 0.67	BA35	311.7 ± 112.5	432.1 ± 93.0	.006	-1.29 ± 1.21		
BA36	1315.8 ± 282.3	1595.5 ± 322.6	.046	-0.87 ± 0.87	BA36	1196.5 ± 402.8	1560.4 ± 329.5	.014	-1.10 ± 1.22		
CS	314.8 ± 105.2	299.5 ± 88.1	.318	0.17 ± 1.19	CS	194.7 ± 86.4	216.5 ± 101.3	.969	-0.22 ± 0.85		
MISC	169.4 ± 35.0	138.1 ± 51.3	.034	0.61 ± 0.68	MISC	176.0 ± 40.0	146.2 ± 49.7	.043	0.60 ± 0.80		

Abbreviations: AD, Alzheimer's disease; ASHS, automatic segmentation of hippocampal subfields; BA, Brodmann area; CA, cornu ammonis; CS, collateral sulcus; DG, dentate gyrus; ERC, entorhinal cortex; MISC, miscellaneous parts; SD, standard deviation; SUB, subiculum.

NOTE. Data are expressed as the means ± SD.

kernel. This value (8 mm) was determined by doubling the full width at half maximum value of the PET scanner (4 mm).

## 2.5. Statistical analyses

For the correlation analyses between subregions and tau/amyloid depositions, we used the data from only the early AD patients because we designed this study to investigate the pathophysiology of AD. We determined the correlation between each subregional volume and PET images with the SPM12 voxelwise regression analyses.

We evaluated correlations using the "multiple regression" design with age, sex, and the intracranial volume calculated by ASHS as nuisance covariates and each subregional volume as the main covariate. For the reciprocal PET comparison between the AD patients and healthy control subjects, we also used SPM12 and a "two-sample *t*-test" design with age and sex as covariates. Correlations or differences that met the following criteria were deemed significant: a

height threshold of  $P < .001$  (uncorrected) and an extent threshold of  $P < .05$  (familywise error).

We also compared the subregional volume changes in the two groups using an analysis of covariance model with age, sex, and intracranial volume as covariates. Statistical Package for Social Science software (version 23.0; Japan, Tokyo) was used and  $P < .05$  was considered significant. To better understand atrophic selectivity in different regions, we also calculated the z-scores of the early AD patients in each subregion using the mean and SD values of the control subjects.

## 3. Results

The calculated volume of each subregion is shown in Table 1. Patients with early AD showed significant atrophy in parts of the hippocampal subfields and in the extrahippocampal cortices. According to the z-scores, in the hippocampus, CA1 and DG showed severe atrophy, whereas CA2 and CA3 were relatively preserved.

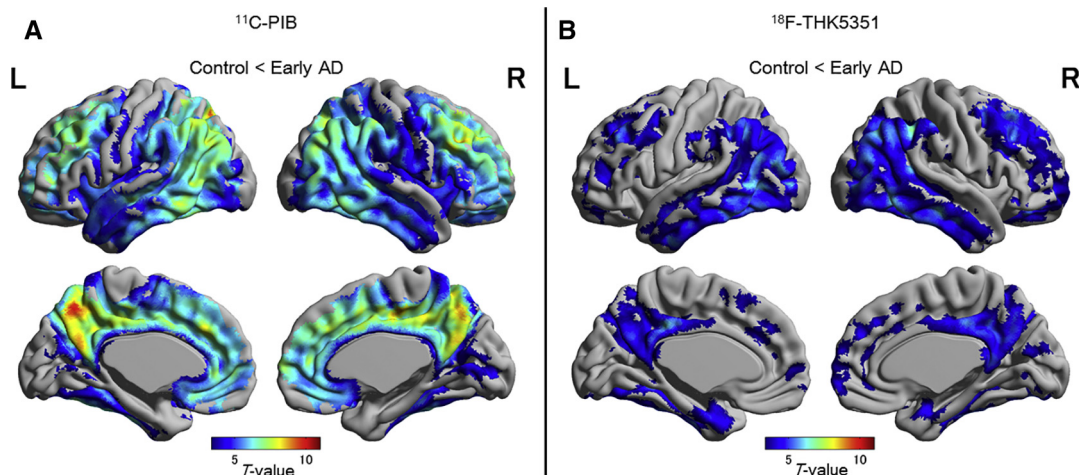


Fig. 1. Significant increases in both (A) <sup>11</sup>C-PIB (left) and (B) <sup>18</sup>F-THK5351 PET (right) uptakes were identified in the early AD group. Abbreviations: AD, Alzheimer's disease; PET, positron emission tomography.

Table 2  
Significant negative correlations between each subregional volume and  $^{18}\text{F}$ -THK5351/ $^{11}\text{C}$ -PIB PET

Subregion	Cluster size (familywise error <i>P</i> value)	<i>T</i> value	<i>x</i>	<i>y</i>	<i>z</i>	Correlative region	BA	
<i><sup>18</sup>F-THK5351 PET</i>								
Right BA35	4886 (.010)	5.19	40	-30	-15	Rt	FG, PHG	20, 36
		5.16	39	-43	-10		FG	37
		4.69	51	-36	-2		MTG	22
Right BA36	8616 (<.001)	6.55	51	-29	-20	Rt	FG, ITG	20
		6.55	38	-34	-20		PHG, FG	20, 36
		5.34	48	-36	-11		FG	37
Left BA36	6726 (.002)	7.19	-46	-46	-22	Lt	FG, ITG	20, 36, 37
		5.77	-38	-32	-14		PHG, FG	20, 36
		5.33	-41	-56	-12		FG	37
	3358 (.031)	6.74	56	-54	-18	Rt	FG	37
		5.00	40	-53	-9		FG	37
		4.89	38	-55	-10		FG	37
<i><sup>11</sup>C-PIB PET</i>								
Right CA3	11,657 (.007)	5.28	45	-54	17	Rt	STG	39
		5.22	45	-30	0		MTG, STG	21, 22
		4.91	49	-79	0		MOG, ITG	18
	8890 (.016)	4.68	27	18	-17	Rt	IFG	47
		4.61	14	27	-24		OFC, IFG, RG	11, 47
		4.59	12	5	-11		Subcallosal	34
	7999 (.022)	5.38	-27	-8	-34	Lt	Uncus	20, 36
		4.99	-50	-44	-21		FG	20, 36
		4.66	-60	-19	-17		ITG	20

Abbreviations: BA, Brodmann area; CA, cornu ammonis; FG, fusiform gyrus; IFG, inferior frontal gyrus; ITG, inferior temporal gyrus; Lt, left; MOG, middle occipital gyrus; MTG, middle temporal gyrus; OFC, orbitofrontal cortex; PET, positron emission tomography; PHG, parahippocampal gyrus; RG, rectal gyrus; Rt, right; STG, superior temporal gyrus.

NOTE. The coordinates are shown on the Talairach atlas. All the unlisted correlations were insignificant.

The early AD patients showed significantly increased uptakes on both  $^{11}\text{C}$ -PIB and  $^{18}\text{F}$ -THK5351 PET (Fig. 1). Although amyloid accumulation was diffusely distributed, it was particularly intense in the posterior cingulate and precuneus areas, as well as the lateral temporal lobes and frontal poles. The tau depositions were also widespread, but they were intense in the inferior lateral temporal lobes.

We also observed significant negative correlations between some of the subregional volumes and the  $^{18}\text{F}$ -THK5351 PET results (Table 2, Fig. 2). The right BA35 and BA36 volumes were significantly associated with the ipsilateral temporal lobar  $^{18}\text{F}$ -THK5351 uptakes, whereas the left BA36 showed significant negative correlations with  $^{18}\text{F}$ -THK5351 in the bilateral temporal lobes. There were no significances in the hippocampal subfields. On the other hand, the  $^{11}\text{C}$ -PIB PET showed relatively broad correlations with the right CA3 volumes (Table 2, Fig. 2).

#### 4. Discussion

Our present findings determined regional tau deposition patterns associated with hippocampal and parahippocampal subregional atrophy and identified significant correlations with tau deposition in extrahippocampal subregional atrophy rather than hippocampal subfields. Judging from the *z*-scores, CA1 or DG as hippocampal subfields showed more severe atrophy extrahippocampal subregions. Given that extrahippocampal atrophy nevertheless had a greater association with

tau deposition, our findings may reflect different mechanisms that are distinct from merely atrophy progression.

According to the hallmark AD pathologic theory [14,15], NFTs, which consist of intraneuronal aggregates of tau, first target the ERC and PRC, damaging the perforant pathway to the hippocampus. Subsequently, the NFTs affect the hippocampus, with the CA1 and subiculum targeted before the CA2 or CA3. In ASHS, BA35 and BA36 account for the PRC [9], which is a part of the memory system [7]. The atrophy of bilateral PRC was less severe than that of the CA1, DG, and ERC (Table 1), but was significantly correlated with broad tau deposition, which is consistent

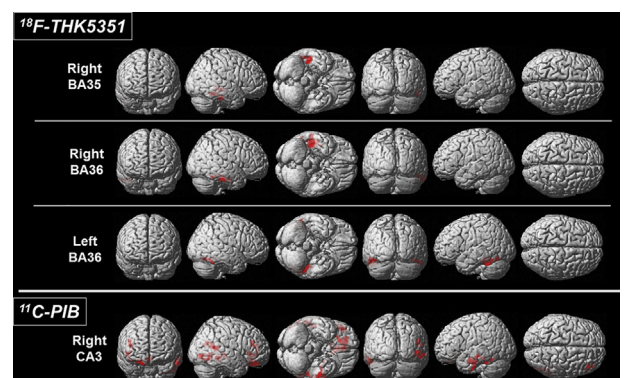


Fig. 2. There were several significant negative correlations between each subregional volume and  $^{18}\text{F}$ -THK5351/ $^{11}\text{C}$ -PIB PET in the early AD group. Abbreviations: AD, Alzheimer's disease; CA, cornu ammonis; BA, Brodmann area; PET, positron emission tomography.

with the pathologic theory, suggesting that these areas are directly related to NFTs. However, hippocampal subfields except the right CA1 may have different and complicated underlying mechanisms of atrophy in AD.

A previous pathologic study revealed significant associations among NFTs, neuronal loss, and cognition, and NFTs in the parahippocampal area were considered the best predictor of the MMSE score [16], although controversy persists regarding whether NFTs are causative or due to a protective process [17]. Because increased tau in cerebrospinal fluid reflects not regional tau deposition, but neuronal damage and disease progression, tau PET is expected to be useful for estimations of regional tau deposition in AD [1]. Thus, the correlations between tau PET and various clinical anatomic parameters should be a fruitful area of investigation. The significant correlations of atrophy levels in several subregions and the locations of relevant tau depositions revealed in the present study contribute to the understanding of AD.

We also found a significant correlation between the right CA3 atrophy and broad amyloid depositions. The right CA3 neuronal loss is considered to have an association with amyloid  $\beta$  and NMDA receptors' functions [18,19], which might be the cause of our results. However, there still remains a question about this result, given that the ASHS showed the lowest performance for CA2/3 segmentation [9] and our patients showed no significant CA3 atrophy as a group comparison (Table 1).

According to pathologic studies, amyloid plaques accumulate mainly in neocortices and are less associated with AD progression and cognitive impairment [14,16], and a recent tau and amyloid PET imaging study confirmed such a tendency [2]. We also found no significant correlations between amyloid deposition and any subregional atrophy. The pathologic process of AD precedes the clinical diagnosis by several years [20], and amyloid deposition may also reach a plateau at diagnosis following such a preclinical stage [21]. On the other hand, our use of  $^{11}\text{C}$ -PIB PET for the diagnosis of AD may possibly have skewed the results about amyloid.

Hippocampal subfields are receiving widespread attention in the neuroimaging of AD [4]. The ASHS software shows reliable concordance with manual segmentation even in the parahippocampal areas [9]. Most studies suggested that CA1 in the hippocampus shows the most severe neuronal loss and strongest associations with cognition and the pathologic stage [22,23], whereas some studies reported significant subiculum and ERC atrophy in AD [23,24]. Our ASHS results also showed volume reductions in these areas, which would be consistent with previous studies. However, the correlations with regional tau deposition varied (Table 2, Fig. 2), suggesting different degenerative mechanisms in each subregion.

The main limitation of this study is the relatively small sample size (18 AD patients and 18 control subjects) and the use of uncorrected  $P$  values for the height threshold and the lack of correction of accumulated alpha errors because of multiple comparisons, which could make our results exploratory or preliminary. We speculate that the extent threshold

with familywise error correction would overcome this shortcoming, and our findings may thus provide additional new knowledge on AD. Moreover, because of potential beta errors, we cannot conclude that there are absolutely no correlations in our insignificant analyses. The lack of genetic data (e.g., *APOE*  $\epsilon 4$  gene) is another limitation, given that such parameters may affect subfield atrophy patterns [24]. In addition, a most recent report has suggested that  $^{18}\text{F}$ -THK5351 PET might bind monoamine oxidase B [25]. We used the cerebellar cortex as the reference, which is considered the least-affected region by this problem [25], and no participant took monoamine oxidase B inhibitors in the present study. However, this issue should be addressed and resolved by future studies.

## 5. Conclusions

Regional tau deposition was correlated with PRC atrophy rather than hippocampal subfields, suggesting different underlying mechanisms of atrophy in early AD. Amyloid deposition showed a correlation with right CA3 atrophy.

## Acknowledgments

This study was supported by the following funding: Brain Mapping by Integrated Neurotechnologies for Disease Studies (Brain/MINDS) project (Grant no. 16dm0207017h0003), the Japan Agency for Medical Research and Development (AMED), and an Intramural Research Grant (27-9) for Neurological and Psychiatric Disorders from the National Center of Neurology and Psychiatry (Japan).

## RESEARCH IN CONTEXT

1. Systematic review: We searched Medline and PubMed databases for studies on in vivo tau positron emission tomography, hippocampal subfields, and relevant pathologic findings in Alzheimer's disease. Relevant studies were additionally found in the reference lists of articles or citation lists on PubMed.
2. Interpretation: We demonstrated that regional tau deposition patterns were associated with extrahippocampal subregional atrophy and not with hippocampal subfields, suggesting different underlying mechanisms of atrophy in early AD. Amyloid positron emission tomography showed a broad correlation only with the right CA3 subfield.
3. Future directions: Further studies including larger and multistage cohorts with the analysis of genetic data would be helpful to determine these correlations and mechanisms more precisely.

## References

- [1] Holtzman DM, Carrillo MC, Hendrix JA, Bain LJ, Catafau AM, Gault LM, et al. Tau: from research to clinical development. *Alzheimers Dement* 2016;12:1033–9.
- [2] Ossenkoppele R, Schonhaut DR, Scholl M, Lockhart SN, Ayakta N, Baker SL, et al. Tau PET patterns mirror clinical and neuroanatomical variability in Alzheimer's disease. *Brain* 2016;139:1551–67.
- [3] Matsuda H. MRI morphometry in Alzheimer's disease. *Ageing Res Rev* 2016;30:17–24.
- [4] Maruszak A, Thuret S. Why looking at the whole hippocampus is not enough—a critical role for anteroposterior axis, subfield and activation analyses to enhance predictive value of hippocampal changes for Alzheimer's disease diagnosis. *Front Cell Neurosci* 2014;8:95.
- [5] Khan W, Westman E, Jones N, Wahlund LO, Mecocci P, Vellas B, et al. Automated hippocampal subfield measures as predictors of conversion from mild cognitive impairment to Alzheimer's disease in two independent cohorts. *Brain Topogr* 2015;28:746–59.
- [6] van Strien NM, Cappaert NL, Witter MP. The anatomy of memory: an interactive overview of the parahippocampal-hippocampal network. *Nat Rev Neurosci* 2009;10:272–82.
- [7] Ranganath C, Ritchey M. Two cortical systems for memory-guided behaviour. *Nat Rev Neurosci* 2012;13:713–26.
- [8] Harada R, Okamura N, Furumoto S, Furukawa K, Ishiki A, Tomita N, et al. 18F-THK5351: a Novel PET radiotracer for imaging neurofibrillary pathology in Alzheimer disease. *J Nucl Med* 2016;57:208–14.
- [9] Yushkevich PA, Pluta JB, Wang H, Xie L, Ding SL, Gertje EC, et al. Automated volumetry and regional thickness analysis of hippocampal subfields and medial temporal cortical structures in mild cognitive impairment. *Hum Brain Mapp* 2015;36:258–87.
- [10] Sone D, Sato N, Maikusa N, Ota M, Sumida K, Yokoyama K, et al. Automated subfield volumetric analysis of hippocampus in temporal lobe epilepsy using high-resolution T2-weighted MR imaging. *Neuroimage Clin* 2016;12:57–64.
- [11] McKhann GM, Knopman DS, Chertkow H, Hyman BT, Jack CR Jr, Kawas CH, et al. The diagnosis of dementia due to Alzheimer's disease: recommendations from the National Institute on Aging-Alzheimer's Association workgroups on diagnostic guidelines for Alzheimer's disease. *Alzheimers Dement* 2011;7:263–9.
- [12] Gonzalez-Escamilla G, Lange C, Teipel S, Buchert R, Grothe MJ. Alzheimer's disease neuroimaging I. PETPVE12: an SPM toolbox for partial volume effects correction in brain PET—application to amyloid imaging with AV45-PET. *Neuroimage* 2017;147:669–77.
- [13] Ashburner J. A fast diffeomorphic image registration algorithm. *Neuroimage* 2007;38:95–113.
- [14] Braak H, Braak E. Neuropathological staging of Alzheimer-related changes. *Acta Neuropathol* 1991;82:239–59.
- [15] Braak H, Braak E, Bohl J. Staging of Alzheimer-related cortical destruction. *Eur Neurol* 1993;33:403–8.
- [16] Giannakopoulos P, Herrmann FR, Bussiere T, Bouras C, Kovari E, Perl DP, et al. Tangle and neuron numbers, but not amyloid load, predict cognitive status in Alzheimer's disease. *Neurology* 2003;60:1495–500.
- [17] Serrano-Pozo A, Frosch MP, Masliah E, Hyman BT. Neuropathological alterations in Alzheimer disease. *Cold Spring Harb Perspect Med* 2011;1:a006189.
- [18] Xu Y, Cao DH, Wu GM, Hou XY. Involvement of P38MAPK activation by NMDA receptors and non-NMDA receptors in amyloid-beta peptide-induced neuronal loss in rat hippocampal CA1 and CA3 subfields. *Neurosci Res* 2014;85:51–7.
- [19] Rammes G, Mattusch C, Wulff M, Seeser F, Kreuzer M, Zhu K, et al. Involvement of GluN2B subunit containing N-methyl-D-aspartate (NMDA) receptors in mediating the acute and chronic synaptotoxic effects of oligomeric amyloid-beta (Aβ) in murine models of Alzheimer's disease (AD). *Neuropharmacology* 2017;123:100–15.
- [20] Morris JC. Early-stage and preclinical Alzheimer disease. *Alzheimer Dis Assoc Disord* 2005;19:163–5.
- [21] Jack CR Jr, Knopman DS, Jagust WJ, Shaw LM, Aisen PS, Weiner MW, et al. Hypothetical model of dynamic biomarkers of the Alzheimer's pathological cascade. *Lancet Neurol* 2010;9:119–28.
- [22] Rossler M, Zarski R, Bohl J, Ohm TG. Stage-dependent and sector-specific neuronal loss in hippocampus during Alzheimer's disease. *Acta Neuropathol* 2002;103:363–9.
- [23] Mueller SG, Schuff N, Yaffe K, Madison C, Miller B, Weiner MW. Hippocampal atrophy patterns in mild cognitive impairment and Alzheimer's disease. *Hum Brain Mapp* 2010;31:1339–47.
- [24] Mueller SG, Weiner MW. Selective effect of age, Apo e4, and Alzheimer's disease on hippocampal subfields. *Hippocampus* 2009;19:558–64.
- [25] Ng KP, Pascoal TA, Mathotaarachchi S, Theriault J, Kang MS, Shin M, et al. Monoamine oxidase B inhibitor, selegiline, reduces 18F-THK5351 uptake in the human brain. *Alzheimers Res Ther* 2017;9:25.